

# **Macroscopic Salt Rejection through Electrostatically Gated Monolayer Porous Graphene**

Roman M. Wyss,<sup>†,§</sup> Tian Tian,<sup>‡,§</sup> Khadija Yazda,<sup>¶</sup> Hyung Gyu Park,<sup>¶</sup> and  
Chih-Jen Shih<sup>\*,‡</sup>

<sup>†</sup>*Institute of Soft Materials Department of Material Sciences, Eidgenössische Technische Hochschule (ETH) Zürich, Vladimir-Prelog-Weg 1-5, Zürich CH-8093, Switzerland.*

<sup>‡</sup>*Institute for Chemical and Bioengineering Department of Chemistry and Applied Biosciences, Eidgenössische Technische Hochschule (ETH) Zürich, Vladimir-Prelog-Weg 1-5, Zürich CH-8093, Switzerland.*

<sup>¶</sup>*Nanoscience for Energy Technology and Sustainability, Department of Mechanical and Process Engineering, Eidgenössische Technische Hochschule (ETH) Zürich, Tannenstrasse 3, Zürich CH-8092, Switzerland.*

<sup>§</sup>*R. M. S. and T. T. contributed equally to this work*

E-mail: chih-jen.shih@chem.ethz.ch

## Abstract

Atomically thin graphene nanopores is emerging as one of the most promising candidates for next-generation membrane technology owing to the ultrahigh permeability. However, the size-exclusive mechanism limits its scalability as it remains technically challenging to drill subnanometer pores over a large area. Here we report macroscopic salt rejection through monolayer porous graphene with the pore sizes of  $20\pm10$  nanometers, overcoming the pore size limitation set by the hydrated radii. By electrostatically gating a sheet of porous graphene, we report a considerable reduction of salt flux by up to 55% with the gate voltage. We systematically investigate the effects of salt concentration and species, including developing a theory to model the electrolyte diffusion through a nanopore in a sheet of gated monolayer graphene. The interplay between graphene quantum capacitance and electrical double layer is identified to be the main mechanism responsible for the observed salt rejection, when the pore size is comparable to the Debye screening length. Our findings reveal a new degree of freedom controlling the membrane potential and electrolyte permeation through porous two-dimensional monolayers.

# Introduction

In the emerging field of nanofluidics, a central objective is to manipulate transport phenomena at nanometer scale to enable new technological opportunities for sensing and energy applications. The reduction of characteristic dimensions in nanofluidics gives rise to substantially different transport properties compared to their bulk counterparts.<sup>1</sup> In nanopores, for example, the effect of surface-mediated transport becomes dominant when the pore size is comparable to the solute diffusion length, enabling new applications, including ionic diodes,<sup>2</sup> field-effect transistors,<sup>3</sup> desalination

cite

, and nanopore-based DNA sequencing,<sup>4,5</sup> Atomically thin two-dimensional (2D) materials, such as graphene, represent an ideal category of membrane materials due to their ultimate permeability.<sup>6</sup> In electrolyte systems, specifically for the aqueous media, early research has suggested that the separation of ions by the pore size differentiating the hydrated radii of  $\sim 1\text{-}3$  nm enables excellent salt rejection

(cite Refs. [1-7] in <https://www.nature.com/articles/ncomms11408.pdf>)

. Nevertheless, the fabrication of sub-5 nanometer porous 2D membranes over a large area with atomic precision is technically challenging<sup>7</sup>

also Refs [8], [9] in the nature comm paper, as well as the nature comm paper itself

. Moreover, a small portion of large pores can significantly diminish salt rejection. To address these issues, recent research efforts have been focused on control over the surface charges by chemical functionalization

cite 7-13

. However, it remains controversial that if the surface charges can result in a degree of salt rejection, as the membrane potential is sensitive to the surroundings and chemical treatment

onecite

. The difficulty in turn hinders fundamental understanding of the interactions between the atomically thin 2D membrane and electrolyte solution. Here, we demonstrate macroscopic salt

rejection through a sheet of large-area porous monolayer graphene using electrostatic gating.

## Results and discussions

### Free diffusion through porous graphene

Figure 1a presents the experimental setup characterizing ionic diffusion through a sheet of monolayer porous graphene (PG). Two reservoirs, namely the high-concentration reservoir (HCR) containing electrolyte solution with molar concentration  $c_0$ , and the low-concentration reservoir (LCR) containing de-ionized (DI) water, are separated by a PG membrane supported by polycarbonate track-etched (PCTE) film. Magnetic stirrers are used to minimize the mass transfer resistance in both reservoirs, and a conductivity probe is placed in the LCR to monitor the ionic concentration as a function of time. The membrane is attached to a piece of copper tape connected to a voltage source applying an electrical bias VG, with the LCR grounded (Figure 1a inset). We fabricated the PCTE-supported PG using the protocol developed by our group

cite

, as schematically shown in Figure 1b. By optimizing the process, a high surface coverage ( $\sim 98\%$ ) of graphene on PCTE was reached (Figure 1c), allowing us to reliably characterize the ion transport behavior (details see Supplementary Information Section S1). The circular pores with pore diameters of  $20 \pm 10$  nm (Figure 1c inset) over a large area were drilled on monolayer graphene. The system presented here allows us to systematically investigate the diffusive flux across a sheet of porous graphene,  $J$ , driven by the gradient of electrochemical potential in the electrolyte medium.

First, the control experiments were carried out by measuring the ionic diffusion of seven salt species, including KCl, NaCl, LiCl, K<sub>2</sub>SO<sub>4</sub>, MgSO<sub>4</sub>, CaCl<sub>2</sub> and K<sub>3</sub>Fe(CN)<sub>6</sub>, through the bare PCTE membrane at  $c_0 = 0.1$  mM. As the diffusive flux is comparably small, the conductivity versus time profile (e.g. Figure 2a) remains linear within the measurement duration ( $\sim 1$  h), suggesting the concentration change in individual reservoirs is negligible

really?

. The diffusive fluxes correspond to different salts were obtained by converting the conductivity-time profiles with the calibration curves (blue bars in Figure 2b and Supplementary Figure S2). On the other hand, for comparison purposes, based on the assumption that the membrane is composed of cylindrical pores with uniform diameter and a low tortuosity  $\tau$  of  $\sim 1.2$

cite 14

, the molar diffusive flux through the bare PCTE membrane,  $J_{\text{PCTE}}$ , follows:

$$J_{\text{PCTE}} = \frac{\pi a^2 N_p D \Delta c}{\delta \tau} \quad (1)$$

where  $a$  is the PCTE pore radius,  $N_p$  is numbers of pore per area,  $D$  is the salt diffusivity, and  $\Delta c$  is the bulk concentration difference between two reservoirs, i.e.,  $\Delta c \sim c_0$ ,  $\delta$  is the thickness of the PCTE membrane, and  $\tau$  is the tortuosity. By using the salt diffusivity values provided by the PTCE vendor (Supplementary Table SX)

ref

), the calculated diffusive fluxes (red bars in Figure 2b) show reasonable agreement with the experimental values.

Next, we carried out the same experiments using the PG-covered PCTE membrane (PG-PCTE), without electrostatic gating. The measured diffusive flux values,  $J_{\text{PG0}}$  (green bars in Figure 2b), remain at the same order of magnitude compared to those of bare PCTE membrane, suggesting that the mass transfer resistance of PG is not significant, as the permeability is high. We observed a more pronounced decrease of diffusive flux in KCl, K<sub>2</sub>SO<sub>4</sub> and K<sub>3</sub>Fe(CN)<sub>6</sub> systems but not for the rest of the salts. We hypothesized that the strong cation- $\pi$  interactions between K<sup>+</sup> cations and graphene

15

slow down the migration of cations along the surface-mediated transport pathway, which has been proven as a strong contributor at low concentration

•  
cite

## Salt rejection induced by electrostatic gating

We next discuss the effects of electrostatic gating on graphene. In order to avoid any interference from the conductivity probe to the membrane potential, the “three-interval” method, which had been used in controlling the membrane potential in mesoporous carbon membranes

8

, is adopted here. Figure 2a presents a representative data of the measured conductivity with respect to time. Specifically, in the first interval, the gate voltage source is turned off and the conductivity probe is on, allowing us to obtain the conductivity-time profile corresponding to the diffusive flux through the PG-PCTE membrane, giving the average slope  $s_1$ . In the second interval, a voltage  $V_G$  is applied to the membrane after turning off the conductivity probe, followed by the third interval, in which the conductivity probe is turned on again to give the corresponding slope,  $s_3$ . The slope corresponding to the second interval,  $s_2$ , as the conductivity probe is off, is determined by linearly interpolating the conductivities from the endpoint of interval 1 to the starting point of interval 3. Accordingly, we define the salt rejection factor,  $\xi$ , which is effectively equivalent to the relative degree of diffusive flux decrease as follows:

$$\xi = \frac{\bar{s} - s_2}{\bar{s}} = \frac{\mathbf{J}_{\text{PG0}} - \mathbf{J}_{\text{PG}}(V_G)}{\mathbf{J}_{\text{PG0}}} \quad (2)$$

where  $\bar{s}$  is the average slope of  $s_1$  and  $s_2$ , namely  $(s_1 + s_2)/2$

Should this be  $(s_1 + s_3)/2$ ?

, and  $\mathbf{J}_{\text{PG}}(V_G)$  is the diffusive flux across the PTCE-supported PG double layer as a function of  $V_G$ . Note that a positive  $\xi$  between 0 and 1 represents a decrease of the diffusive flux. The factor  $\xi$  enables a reliable and stable measurement of salt rejection, as the salt species and initial conditions may induce a degree of measurement uncertainty between different samples. A con-

trol experiment was performed to ensure the copper tape was not in direct contact with the ionic solution (Supplementary Section 3).

Using 0.1 mM KCl solution in HCR, we measured  $\xi$  as a function of  $V_G$  within  $\pm 1.25$  V, before triggering the electrochemical reactions (Figure 2c). We observe an asymmetric dependence of  $\xi$  with respect to  $V_G$ , with a higher degree of salt rejection for  $V_G > 0$ , where positive carriers (holes) are induced in graphene. We notice that an increase  $\xi$ , or a decrease of  $J_{PG}$  with  $V_G$ , showing an inverse trend compared to those observed in ionic field effect transistors (IFETs), in which the diffusive flux increases with the gate voltage. A further increase of the KCl concentration  $c_0$  influences the attainable degree of salt rejection.  $\xi$  values measured at  $V_G=1.25$  V,  $\xi_{\max}$ , as a function of  $c_0$  from  $10^{-4}$  to  $10^{-2}$  M KCl (see Supplementary Section S4) exhibit a power law dependency (Figure 2d). The  $\xi_{\max} - c_0$  relation can be nicely fitted by a power law function following  $\xi_{\max} c_0^{0.59} = \text{Const.}$  As the Debye screening length in solution,  $\lambda_D$ , is inversely proportional to  $c^{0.5}$ , we infer that the  $V_G$ -induced salt rejection originates from the modulation of the electrical double layer (EDL), as will be discussed later.

## Self-consistent ion transport theory

In order to quantitatively understand the observed  $V_G$  dependence, we develop a theory to model the coupling of graphene's elementary transport properties and EDL, in order to quantify the ionic transport through a graphene nanopore. Under the assumption that the time scale for the bulk concentration change is significantly longer than that of ionic diffusion, the pseudo-steady state approximation holds. Accordingly, the steady-state Nernst-Planck equation describing the ionic transport in an electrolyte solution is given by :

$$\nabla \cdot \mathbf{J}_i = -\Delta \cdot \left( \frac{D_i}{k_B T} c_i N_A \nabla \mu_i \right) = 0 \quad (3)$$

where  $\mathbf{J}$  is the mass flux, subscript  $i$  corresponds to the species (anion or cation),  $D$  is the diffusivity,  $k_B$  is the Boltzmann constant,  $T$  is temperature,  $c$  is the molar concentration,  $N_A$  is the

Avogadro constant, and  $\mu_i$  is the electrochemical potential. Under the assumption of ideal solution, it follows : [cite](#)

$$\nabla \mu_i = k_B T \nabla \ln x_i + z_i e \nabla \psi \quad (4)$$

where  $x$  is the molar fraction,  $z$  is the ionic valence,  $e$  is the unit charge, and  $\psi$  is the electric potential. On the other hand, the Poisson equation describing the electric potential distribution is given by:

$$\nabla \cdot (\varepsilon_m \varepsilon_0 \nabla \psi) = -N_A e \sum_i c_i z_i \quad (5)$$

where  $\varepsilon_m$  is the relative permittivity of individual materials in the system. Including water and the internal Stern layer, and  $\varepsilon_0$  is the vacuum permittivity. When applying  $V_G$  to graphene adjacent to the electrolyte solution, charges (electrons or holes) are induced in graphene; the electroneutrality of the entire system suggests: [for graphene?](#)

$$\sigma_G S_G + \sum_i \int_{\Omega} z_i c_i N_A e d^3 \Omega = 0 \quad (6)$$

where  $\sigma_G$  is the charge density in graphene,  $S_G$  is the total area of graphene, and  $\Omega$  corresponds to the entire volumetric domain of electrolyte solution. Note that the graphene surface potential,  $\psi_G$ , is not equivalent to  $V_G$  due to the graphene quantum capacitance effect (Figure 3a) following: [cite-24](#)

$$V_G = \Delta \phi_G + \psi_G \quad (7)$$

where  $\Delta \phi_G$  is the change of graphene's work function. Under the assumption that the charge neutrality point of graphene coincides with the Dirac point at  $V_G = 0$ , the elementary electronic properties of graphene give:

$$\Delta \phi_G = \text{sign}(\sigma_G) \frac{\hbar v_F}{e} \sqrt{\frac{\pi |\sigma_G|}{e}} \quad (8)$$

where  $\hbar$  is the reduced Planck constant, and  $v_F = 1.1 \times 10^6 \text{ m}\cdot\text{s}^{-1}$  is the Fermi velocity of graphene (more details find Supplementary Section SXX ). Note that the PG film fabricated experimentally [ref] is double-layer turbostratic graphene, in which we assume the  $\Delta\phi_G - \sigma_G$  dependence follows Eq. 8. The theory proposed here was solved self-consistently by discretizing Eqs. 3-5 using the finite-element method, in which the graphene surface potential is coupled with Eqs. 6-8 that were solved simultaneously to reach convergent numerical solutions of  $\sigma_G$  and  $\psi_G$  for a given  $V_G$ . Clearly, the above model yields symmetric characteristics for  $\sigma_G$  and  $\psi_G$  with respect to  $V_G$  due to the symmetric band structure of graphene (Eq. 8). However, for chemical vapor deposition-(CVD) synthesized graphene used in our experiments, it is well-recognized that the electron traps are inherently introduced during synthesis and patterning , effectively increasing the graphene [25] quantum capacitance for  $V_G < 0$  (Supplementary Figure SXX ). With the nonideality in mind, [ref] hereafter, we compare the calculations and experiments in the regime of  $V_G > 0$ . For example, Figure 3c presents the calculated  $\sigma_G$  and  $\psi_G$  as a function of  $V_G$  considering the ionic diffusion through a single 20 nm-diameter nanopore drilled on a sheet of semi-infinite double layer graphene that separates HCR containing KCl solution at  $c_0 = 0.1 \text{ mM}$ , and LCR at  $c_0/10$  in axisymmetric coordinates (details see Supplementary Section SXX ). Indeed, the interplay between graphene [cite] quantum capacitance and the EDL significantly reduces the graphene surface potential  $\psi_G$  to  $\sim 0.3 \text{ V}$  at  $V_G = 1.25 \text{ V}$ , corresponding a surface charge density  $\sigma_G$  of  $\sim 0.08 \text{ C}\cdot\text{m}^{-2}$ . Note that as we mentioned earlier, an important merit of the system here is that the surface charge density can be precisely determined and controlled, rather than being treated as a fitting parameter as in most of the 2D nanopore studies, . [cite 18]

## Salt rejection mechanism

The numerical procedure described above allows us to resolve the concentration and electric potential profiles near to a graphene nanopore for a given  $V_G$ . Since the ionic flux is driven by both  $\psi$  and  $c$  fields (see Eq. 3 and 4), we focus on the electrochemical potential  $\mu_i$ , which represents the combined driving force, to reveal its dependence on the applied  $V_G$ . Following the same

system considered in Figure 3b, the calculated axisymmetric electric potential  $\psi$  and the relative electrochemical potentials,  $\Delta\mu_{K^+}$  and  $\Delta\mu_{Cl^-}$ , for  $V_G = 0.75$  V are shown in Figure 4a and 4b, respectively.

say somthing

The reference point of the electrochemical potentials is set at the bulk phase in the HCR. As expected, the electric potential reaches the maximum at the graphene surface (with  $\psi_G$  of  $\sim 100$  mV) and decays towards the bulk solution phase, forming an EDL surrounding the graphene surface. Since the Debye screening length  $\lambda_D$  is comparable to the pore radius  $R_G$ , the electric potential at the nanopore center remains at  $\sim 25$  mV, comparable to the thermal energy at room temperature ( $k_B T = 26$  meV). Consequently, it is evident that the potential barrier is sufficient to modulate the diffusive flux.

We further reveal the cation and anion transport pathways by looking into their electrochemical potentials (Figure 4b). By increasing  $V_G$ , a more positive  $\psi_G$  on graphene surface reduces the cation concentration at the pore edge due to the electrostatic interactions, thereby increasing its concentration gradient at the pore center. On the other hand, the anion concentration near the pore edge increases exponentially, such that the concentration gradient at the pore center becomes small. The observation confirms the distinct ionic transport pathways upon applying a positive  $V_G$ : pore center for cations and pore edge for anions. Figure 4c presents the calculated z-component of the cation and anion fluxes through the pore at the graphene plane ( $z = 0$ ),  $J_z$ , as a function of the normalized radius,  $r/R_G$ , where  $r$  is the radial coordinate and  $R_G$  is the pore radius, at different  $V_G$  values. Note that  $J_z$  is negative because the LCR is placed at  $z \downarrow 0$  in the simulations. At  $V_G = 0$  (pure diffusion), the anion and cation flux profiles are identical, with a higher flux near the pore edge, which is expected, as the concentration gradient is higher. By gradually increasing  $V_G$ , both fluxes are reduced throughout the pore, while the degree of reduction is more pronounced at the pore edge for the cation, and at the pore center for the anion, following the scenarios we discussed above. Accordingly, the integrated fluxes across the pore,  $|J_z|$ , are reduced with  $V_G$  (Figure 4d). A total flux reduction of up to 80% is predicted. Another interesting finding here is that, by increasing

$V_G$ , the nanopore transport preferentially allows cations over anions, or in other words, the anion flux is more reduced with  $V_G$  (see Figure 4c), known as the ion selectivity of graphene nanopore .  
cite 18

The above mechanistic findings, nevertheless, do not fully clarify the experimentally observed reduction of diffusive flux upon gating. Indeed, the same physical mechanism also governs the ionic transport through an IFET, in which a nonzero electric potential at the nanopore center usually results in an increase of ionic conductivity . To this end, we further increased the graphene surface potential  $\psi_G$  considering the same system (Supplementary Section 6 ). Intriguingly, by increasing  $\psi_G$  larger than 400 mV, the ionic flux starts to increase, reversing the trend observed at the low  $\psi_G$  regime, because of an increase of cation diffusion . This level of  $\psi_G$  cannot be reached experimentally in graphene membrane, as this requires a  $V_G$  larger than 2.0 V , which triggers the electrochemical reactions. On the other hand, in an IFET, the electric potential on the pore wall is considerably higher, equivalent to  $V_G$  due to the metallic nature of gate electrode (having an infinitely-large quantum capacitance). We therefore conclude that the quantum capacitance-induced nonlinear damping in the surface potential results in the observed salt rejection. Following the above discussions, we further investigate the physical limits for the biased graphene nanopores. Specifically, the salt rejection characteristics are controlled by: (i) the overlap of EDL inside the nanopore, essentially controlled by two length scales of  $\lambda_D$  and  $R_G$ , and (ii) the graphene surface potential  $\psi_G$  controlled by  $V_G$  following Eq. 7. To this end, we calculate  $\psi_G$  as a function of  $\lambda_D/R_G$  and  $V_G$  (Figure 5a). Clearly, when the bulk concentration  $c_0$  increases, a higher  $V_G$  is required to reach the same level of  $\psi_G$ . Consequently, as revealed in Figure 5b, the calculated salt rejection factor  $\xi$  increases with both  $\lambda_D/R_G$  and  $V_G$ , in line with the experimentally observed  $\xi - c_0$  dependence. We also find the overall trends for  $\psi_G$  and  $\xi$  with respect to  $\lambda_D/R_G$  and  $V_G$  are very similar. More importantly, based on our theoretical prediction, with  $V_G=1.25$  V and  $\lambda_D/R_G=1.0$ , a high value of  $\xi$  of  $>0.85$  can be achieved.

## Effects of salt species

Finally, we examine other salt species and compare the degree of salt rejection between experiments and simulations. Figure 6a presents the measured salt rejection  $\xi$  as a function of  $V_G$  from at  $c_0=0.1$  mM, for the seven salt species considered here, including NaCl, LiCl, KCl, MgSO<sub>4</sub>, CaCl<sub>2</sub>, K<sub>2</sub>SO<sub>4</sub>, and K<sub>3</sub>Fe(CN)<sub>6</sub> (details see Supplementary Section S7). Similar to the KCl system discussed earlier, the salt rejection was only observed in the positive  $V_G$  regime. The degree of salt rejection decreases with the salt valence; for example, the measured  $\xi$  values at  $V_G=1.25$  V decreases from >0.5 for monovalent NaCl to -0.04 for multivalent K<sub>3</sub>Fe(CN)<sub>6</sub>. This observation is endorsed by our simulations, in which we calculate  $\xi$  as a function of  $V_g$  using the same setups in simulations (Figure 6b; details see Supplementary Section SX). The calculated  $\xi_{\max}$  values are quantitatively compared with experiments (Figure 6c), and the same trend is observed. Indeed, because the Debye screening length  $\lambda_D$  decreases with the salt valence, the graphene surface potential appears to decrease in the multivalent salt systems, thereby reducing  $\xi$  (see Figure 5b). The calculated and experimental  $\xi_{\max}$  as a function of  $\lambda_D$  are consequently plotted, for the seven salt species considered here (Figure 6d). We notice that without any fitting parameters, our theory can predict the experimental values reasonably well. In addition, the  $\xi_{\max} - \lambda_D$  dependence is approximately linear, suggesting that the effect of salt diffusivity is negligible. This finding also explains the concentration dependence of  $\xi_{\max}$  observed in Figure 2d, as  $\delta_D \propto c_0^{-0.5}$ .

## Conclusion

In summary, we have presented a comparative experimental and modeling study on macroscopic salt rejection through a sheet of large-area porous graphene under electrostatic gating. We show that due to a small quantum capacitance of double layer graphene, the graphene surface potential is considerably lower than the applied gate voltage. As a result, the subtle redistribution of the electrochemical potentials create new pathways for ionic transport, which in turn lead to a considerable degree of salt rejection. We report a high degree of salt rejection at  $V_G=1.25$  V of up to 55%

and 80%, based on our experiments and theoretical predictions, respectively. We demonstrate that the observed salt rejection positively correlates with the Debye screening length that nonlinearly modulates the graphene surface potential and charge density. The experimental results and fundamental principles presented here open an avenue towards realization of atomically thin 2D porous membranes for advanced separation process in electrolyte solutions.

## Methods

## References

- (1) Schoch, R. B.; Han, J.; Renaud, P. *Rev. Mod. Phys.* **2008**, *80*, 839–883.
- (2) Karnik, R.; Duan, C.; Castelino, K.; Daiguji, H.; Majumdar, A. *Nano Lett.* **2007**, *7*, 547–551.
- (3) Nam, S.-W.; Rooks, M. J.; Kim, K.-B.; Rossnagel, S. M. *Nano Lett.* **2009**, *9*, 2044–2048.
- (4) Heerema, S. J.; Dekker, C. *Nat. Nanotechnol.* **2016**, *11*, 127–136.
- (5) Garaj, S.; Liu, S.; Golovchenko, J. A.; Branton, D. *Proc. Natl. Acad. Sci.* **2013**, *110*, 12192–12196.
- (6) Cohen-Tanugi, D.; Grossman, J. C. *Nano Lett.* **2012**, *12*, 3602–3608.
- (7) Suk, M. E.; Aluru, N. R. *J. Chem. Phys.* **2014**, *140*, 084707.

## Figures

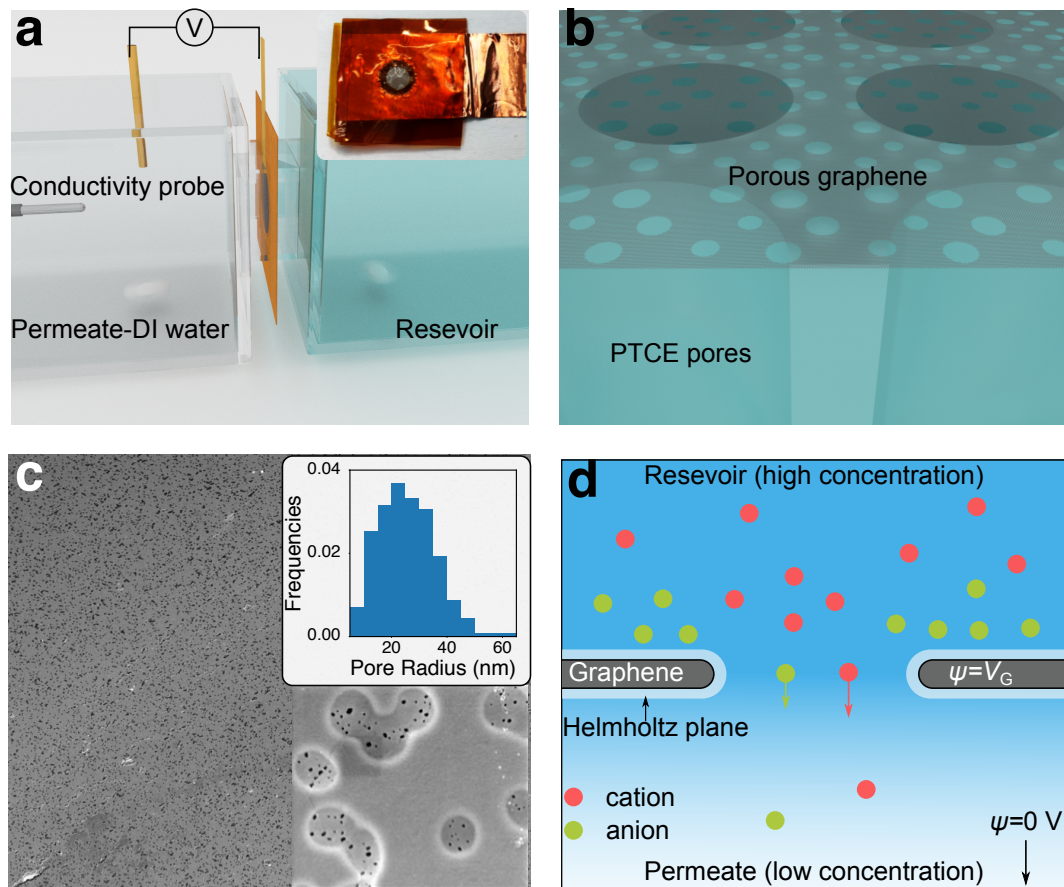


Figure 1: a

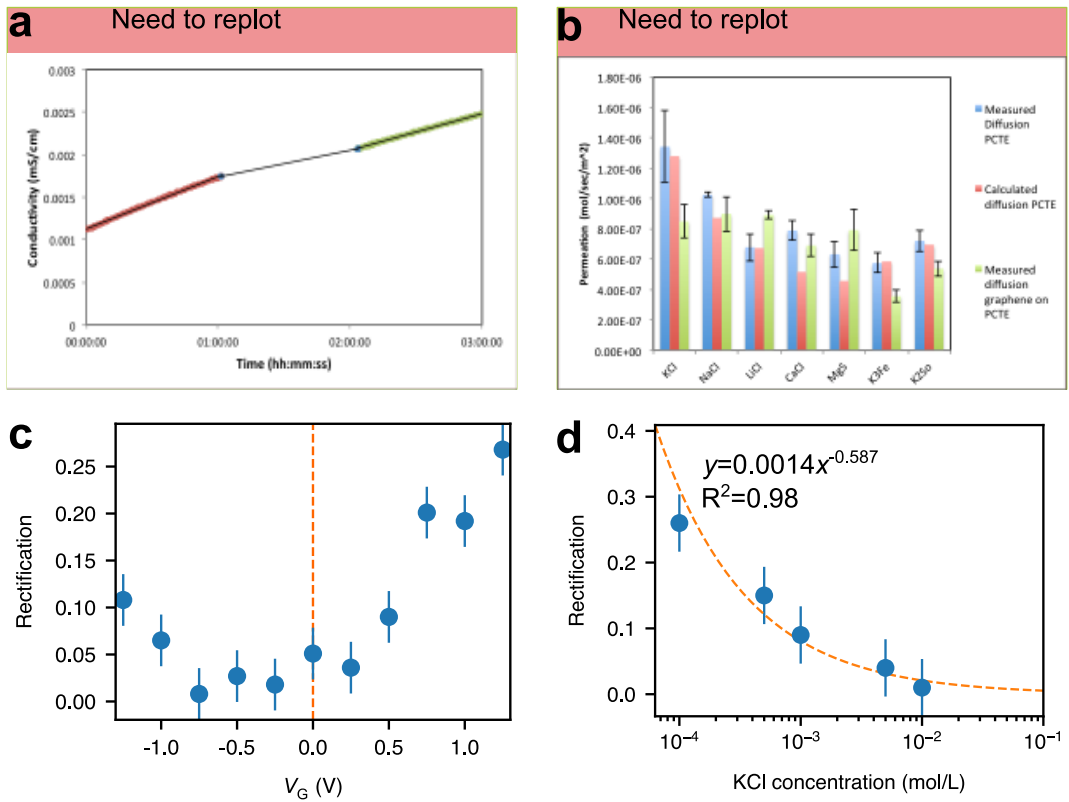


Figure 2: a

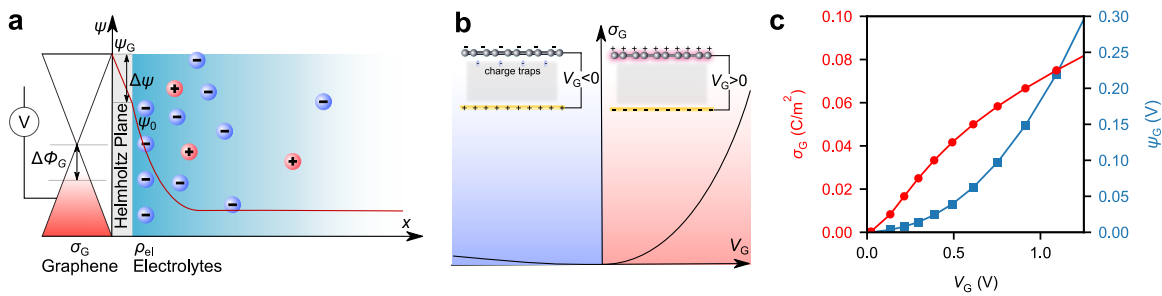


Figure 3: a

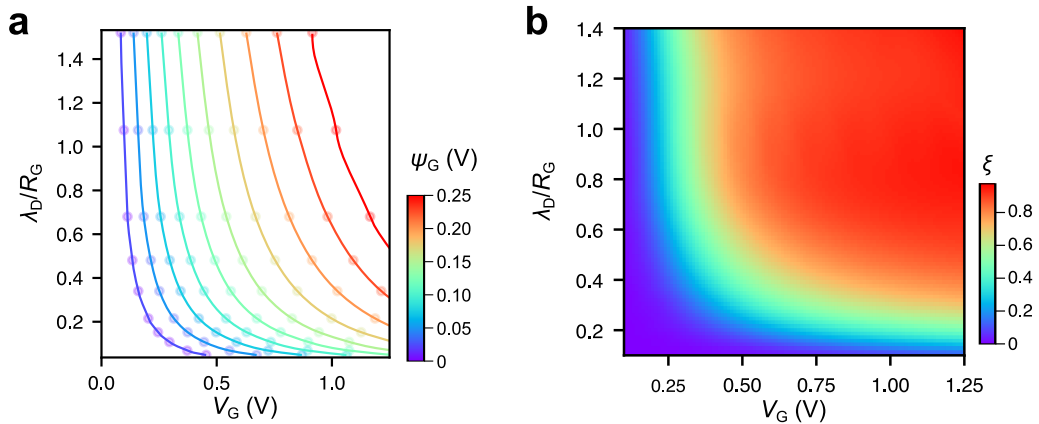


Figure 4: a

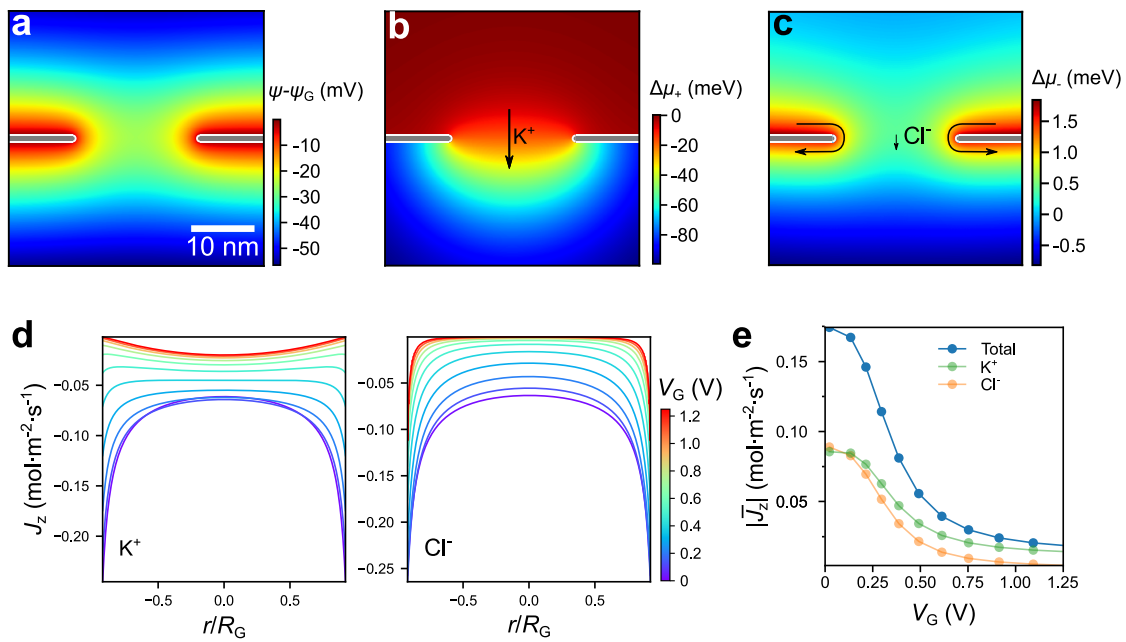


Figure 5: a

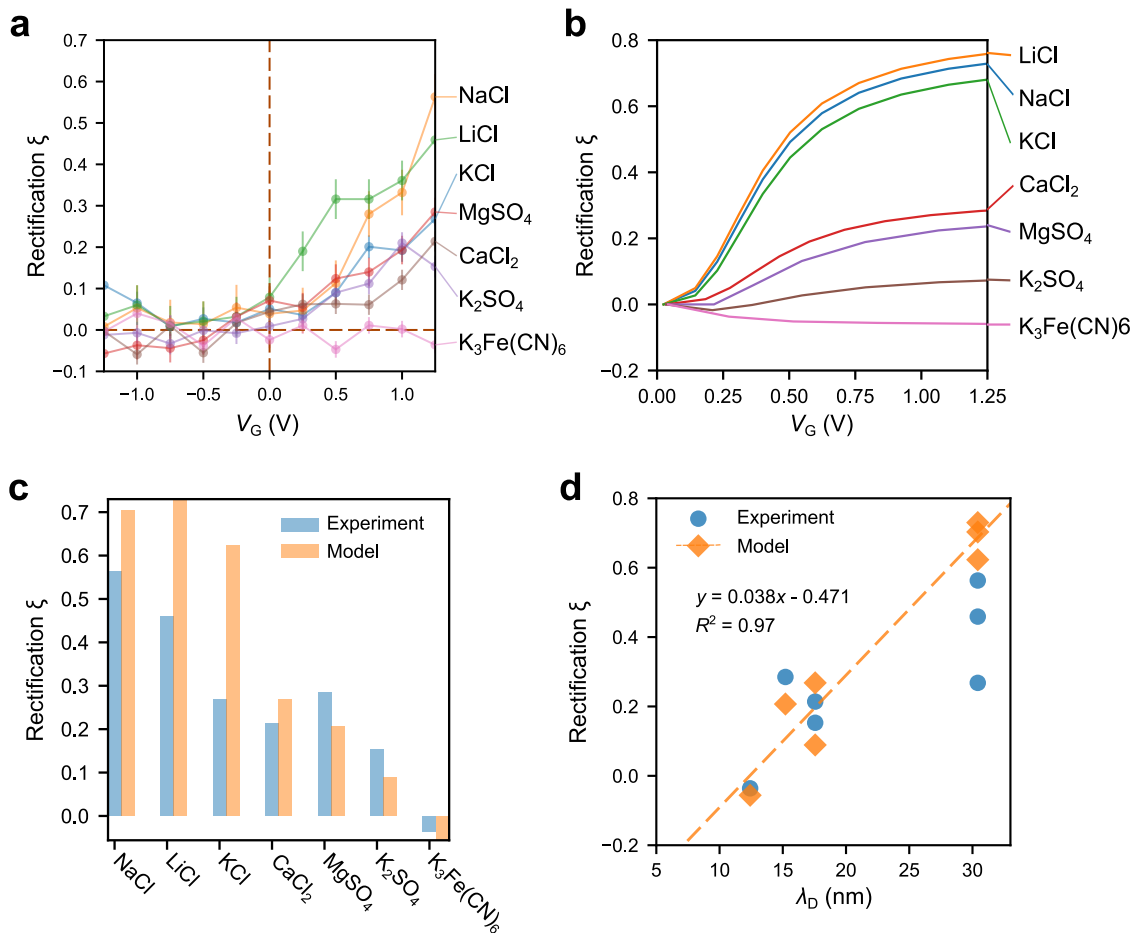


Figure 6: a